[CANCER RESEARCH 62, 7083–7092, December 1, 2002]

A Quantitative Analysis of Rate-limiting Steps in the Metastatic Cascade Using Human-specific Real-Time Polymerase Chain Reaction[1]

Andries Zijlstra, Rebecca Mellor, Giano Panzarella, Ronald T. Aimes, John D. Hooper, Natalia D. Marchenko,[2] and James P. Quigley[3]

Department of Cell Biology, The Scripps Research Institute, La Jolla, California 92037

ABSTRACT

A quantitative assessment of rate-limiting steps in metastasis has always been challenging because of the difficulty of detecting small tumor cell populations. We have developed a highly sensitive assay for monitoring the metastatic dissemination of human tumor cells in the chick embryo and used this assay to investigate the relative efficacy of sequential stages in the metastatic cascade for two malignant human tumor cells lines, HEp3 and HT1080. This assay is based on the real-time PCR amplification of human *alu* sequences and exhibits a high sensitivity (25 cells/lung) with a large linear range (50–100,000 cell/lung). The assay is optimized for a high number of replicate *in vivo* assays (50–100 animals/assay) and can be applied in both experimental and spontaneous metastasis models. Using quantitative *alu* PCR, we determined that HEp3 spontaneously metastasizes very efficiently and rapidly, generating secondary growth in the lung exceeding 1–2 × 10^4 cells/lung in 7 days. In contrast, spontaneous HT1080 metastasis is 50–100-fold less efficient, resulting in only 200–400 cells/lung in 7 days. By taking advantage of the sensitivity and specificity of the real-time *alu* PCR assay we were also able to quantitatively assess multiple steps in metastasis including intravasation, arrest of tumor cells in secondary organs of the embryo, and the initial growth and expansion of the arrested tumor cells. A comparative analysis of HEp3 and HT1080 metastasis demonstrates that the relatively low-to-moderate metastatic rate of HT1080 is caused by two distinct deficiencies, an 8–10-fold lower rate of intravasation and a delayed onset of HT1080 growth expansion in the secondary organ. Thus, a very facile metastasis model system coupled with the sensitive, real-time PCR-based assay allows for the identification and quantification of rate-limiting steps in the metastatic cascade for select human tumor cell lines.

INTRODUCTION

Metastatic dissemination of a neoplasia to secondary sites is the primary cause of death among cancer patients (1–3). Both experimental investigations and clinical observations have established that, in order for a tumor cell to hematogenously disseminate, it must intravasate into the circulation, arrest at a secondary site, and initiate secondary growth (1, 2, 4–8). The sequential nature of this metastatic cascade implies that failure to complete even one of these steps eliminates the possible development of secondary colonization. This theory is corroborated by both clinical and laboratory observations that demonstrate that metastasis is inherently inefficient (9–13). An understanding of the relative contribution of each progressive stage in this metastatic cascade to the overall efficiency of metastatic dissemination would provide critical insight into the rate-limiting steps of metastasis.

Several animal models have been developed to investigate the metastatic properties of human tumor cells. The study of human tumor cell metastasis requires the use of an immunodeficient animal model, such as severe combined immunodeficient mice or avian embryos, and an effective end point assay in which the secondary growth can be assessed, such as morphometric quantitation of lung colonies. Previous quantitative observations, in separate investigations with distinct models, have indicated that the effective success of each step in the metastatic cascade can vary depending on the tumor-cell gene expression profile (14–18) as well as the interactions of the host microenvironment with the tumor cells (7, 12, 19–21) However, to date, very little is known about the relative contribution of individual steps in the cascade to the overall success of metastasis. This is in great part because of the lack of a model that allows for the high throughput of samples required for quantitative studies, as well as the absence of an assay that can quantitatively assess subtle changes in the tumor-cell population within secondary organs.

The chick embryo model has long been used for the investigation of angiogenesis and oncogenesis (22–25). However, the many innovative studies of L. Ossowski [Kim *et al.* (4), Yu *et al.* (16), Ossowski and Reich (26)], and also A. Chambers [Koop *et al.* (15), Chambers *et al.* (27), McDonald *et al.* (28)] have established the chick embryo as a useful model for the investigation of tumor cell metastasis. This model offers many advantages including: (*a*) a naturally immunodeficient host that accepts transplantation from various tissues and species and is amenable to both experimental as well as spontaneous metastasis; (*b*) extra-embryonic membranes that are connected to the embryo through a continuous circulatory system and that are readily accessible for experimental manipulation and observations; and (*c*) a comprehensive *in vivo* experimental system that recapitulates all of the steps in the metastatic cascade and is neither expensive nor time- or labor-intensive. Several methods for semiquantitative analysis of metastasis in the chick embryo have been developed including morphometric assessment of individual metastasized cells (26, 29), selective outgrowth of metastasized cells (27), detection of microscopic tumor colonies (28), and the detection of human uPA[4] activity (26, 30). Because the duration of the assay is limited to a 7–9- day window available before the chick hatches, most tumor cells cannot produce macroscopically visible colonies in secondary organs before the termination of the assay. As a result, the more difficult detection of micrometastases becomes an inherent part of the chick model system.

The analysis of individual tumor cells in tissue extracts by phase-contrast microscopy and the detection of fluorescently labeled tumor cells in intact tissues by video-microscopy has made possible a direct morphometric quantitation of individual cells and micrometastases (28). Although the use of the latter methodology has extended semiquantitative analysis of metastasis to a broader spectrum of tumor cells, this process remains labor-intensive and is restricted to analysis of the organ surface using specialized video microscopic equipment. The quantitative detection of human uPA activity within secondary organs of the embryo (26, 30) is a convenient method but is limited to

Received 6/11/02; accepted 10/4/02.

The costs of publication of this article were defrayed in part by the payment of page charges. This article must therefore be hereby marked *advertisement* in accordance with 18 U.S.C. Section 1734 solely to indicate this fact.

[1] Supported by NIH Grants CA65660, CA55852, and HL31950 (to J. P. Q.) and Training Grant T32 HL07695 (A. Z.), and by a National Health and Medical Research Council of Australia C. J. Martin/R. G. Menzies Fellowship (to J. D. H.).

[2] Present address: The Burnham Institute, 10901 North Torrey Pines Road, La Jolla, CA 92037.

[3] To whom requests for reprints should be addressed, at Department of Cell Biology, The Scripps Research Institute, 10550 North Torrey Pines Road, La Jolla, CA 92037. Phone: (858) 784-7108; Fax: (858) 784-7333; E-mail: jquigley@scripps.edu.

[4] The abbreviations used are: uPA, urokinase-type plasminogen activator; GFP, green fluorescent protein; CAM, chorioallantoic membrane; GAPDH, glyceraldehyde-3-phosphate dehydrogenase; chGAPDH, chicken GAPDH.

metastasizing cells that express moderate to high levels of uPA. Although each of these methods allow the investigator to determine whether metastasis has occurred, their limited sensitivity restricts studies to the analysis of highly metastatic tumor cells and limits the quantitation of multiple metastatic events.

Recently, PCR-mediated amplification of human specific-*alu* sequences was used for semiquantitative detection of intravasated tumors cells in the lower CAM of the chick embryo (4). We have adopted and modified this approach to develop a highly sensitive, real-time PCR based system that allows for the quantitative detection of human cells in all of the chick organs. With real-time *alu* PCR, the detection of metastasized cells over a linear range of 5×10^1 – 1×10^5 cells/lung is made possible for the analysis of experimental as well as spontaneous metastasis. Furthermore, the sensitivity and range of *alu* PCR allows for the analysis of individual steps in the metastatic cascade, including the early events in metastasis (intravasation and arrest) as well as the subsequent growth of secondary colonies. The present study characterizes the quantitative *alu* PCR assay and implements this methodology for the end point analysis of metastasis by several human tumor cell lines. More importantly, however, the relative contribution of intravasation, arrest, and growth to the total metastatic dissemination of human tumor cells is assessed, and the identity of multiple rate-limiting steps in metastasis is presented.

MATERIALS AND METHODS

Cell Culture

HT1080, (fibrosarcoma), A549 (lung carcinoma), HeLa (cervical carcinoma), WI38 (human embryo lung fibroblasts), and Hs746t (gastric carcinoma) were obtained from the American Type Culture Collection (Manassas, VA). HEp3 (epidermoid carcinoma) cells including the M+ and M− variants were obtained as described previously (26, 30–32). MDA MB 435–4A4 (breast carcinoma) cells were a kind gift from Dr. D. Tarin (University of California-San Diego Cancer Center, La Jolla, CA). Cells were cultured in DMEM (Life Technologies, Inc., Gaithersburg, MD) supplemented with 10% FCS (HyClone, Logan, UT). Cell cultures were maintained at 37°C in 5% CO_2/95% air and passaged at confluence. GFP-expressing cell lines were generated by transducing cultured cells with the retroviral vector plEGFP from Clontech (Palo Alto, CA) according to the company's instructions.

Chick Embryo Metastasis Assay

Spontaneous Metastasis. Fertilized White Leghorn eggs (SPAFAS, Storrs, CT) were incubated in a rotary incubator at 38°C with 60% humidity for 10 days. At this time, the CAM was dropped by drilling a small hole through the eggshell into the air sac and a second hole near the allantoic vein that penetrates the eggshell membrane but not the CAM. The CAM is dropped by applying a mild vacuum to the hole over the air sac. Subsequently, a cutoff wheel (Dremel, Racine, WI) was used to cut a square 1-cm^2 window encompassing the second hole near the allantoic vein to expose the underlying CAM. Cultured human cells were detached by trypsinization, washed with complete medium and resuspended in serum free DMEM. Before a 25-μl inoculum of $0.25–1 \times 10^6$ tumor cells was added, the CAM was gently abraded with a sterile cotton swab to provide access to the mesenchyme. The windows were subsequently, sealed and the eggs were returned to a stationary incubator. The eggs remained in the incubator for 1–7 days, after which the extra-embryonic tumor and CAM, as well as the embryonic lung, were harvested and analyzed for the presence of tumor cells by quantitative *alu* PCR as described below. In some experiments, a 50-mg wet weight of other intra-embryonic organs was harvested and analyzed in parallel with the lung. A schematized version of the spontaneous metastasis assay is illustrated in Fig. 1.

Experimental Metastasis and Analysis of Secondary Growth. Fertilized White Leghorn eggs were incubated as described above for 12 days. Before the injection of cultured cells, the allantoic vein was exposed by removing the overlaying eggshell and by rendering the eggshell membrane transparent with a drop of mineral oil. Cultured cells were detached using nonenzymatic cell-dissociation solution, washed, and resuspended in serum-free DMEM at 40×10^6 cells/ml. After delivering $0.5–5 \times 10^5$ cells in 100 μl into the allantoic vein of each embryo, the eggs were returned to a stationary incubator and remained there for an additional 1–7 days. At distinct time points, the lung or lower CAM was harvested from each embryo, as described below, and was processed for the detection of tumor cells.

Intravasation. The ability of tumor cells to intravasate from the primary tumor into the circulation was assessed by the detection of human tumor cells in the lower CAM as described previously (4). In brief, suspensions of tumor cells were applied to the CAM through a 1-cm^2 window cut in the eggshell, as described above for spontaneous metastasis. At indicated time points, the upper portion of the eggs, including the upper portion of the CAM, was removed and the embryo and yolk were decanted so as to expose the lower CAM. Using a 1-cm internal diameter brass cork borer, we collected two separate portions of the CAM, which accounted for approximately 1/10 of the lower CAM (1.6-cm^2), from each embryo. The two sections of the lower CAM were combined and genomic DNA that was extracted from these tissues was analyzed for the presence of human tumor cells.

Quantitative Detection of Human Tumor Cell Metastasis

The detection of human tumor cells in chick lung was based on the quantitative detection of human *alu* sequences present in chick lung DNA extracts and is a modification of the method developed by Kim *et al.* (4). Genomic DNA was extracted from harvested tissues using the Puregene DNA purification system (Gentra Systems, Minneapolis, MN). To detect human cells in the chick tissues, primers specific for the human *alu* sequences (sense: 5′ ACG CCT GTA ATC CCA GCA CTT 3′; and antisense: 5′ TCG CCC AGG CTG GAG TGC A 3′) were used to amplify the human *alu* repeats present in genomic DNA that was extracted from chick tissues. The real-time PCR used to amplify and detect *alu* sequences contained 30 ng of genomic DNA, 2 mM $MgCl_2$, 0.4 μM each primer, 200 μM DNTP, 0.4 units of Platinum Taq polymerase (Invitrogen Corporation, Carlsbad, CA), and a 1:100,000 dilution of SYBR green dye (Molecular Probes, Eugene, OR). Each PCR was performed in a final volume of 10 μl under 10 μl of mineral oil with the iCycler iQ (Bio-Rad laboratories, Hercules, CA) under the following conditions: polymerase activation at 95°C for 2 min followed by 30 cycles at 95°C for 30 s, 63°C for 30 s, and 72°C for 30 s. A quantitative measure of amplifiable chick DNA was obtained through amplification of the chick GAPDH genomic DNA sequence with chGAPDH primers (sense: 5′ GAG GAA AGG TCG CCT GGT GGA TCG; antisense: 5′ GGT GAG GAC AAG CAG TGA GGA ACG) using the same PCR conditions described for *alu*. The fluorescence emitted by the reporter dye was detected online in real-time, and the threshold cycle (*Ct*) of each sample was recorded as a quantitative measure of the amount of PCR product in the sample. The *Ct* is the fractional cycle number at which the fluorescence generated by the reporter dye exceeds a fixed level above baseline. When indicated, the *alu* signal was normalized against the relative quantity of GAPDH and expressed as $\Delta Ct = (Ct_{GAPDH} - Ct_{alu})$. The changes in *alu* signal relative to the total amount of genomic DNA (and, hence, changes in the quantity of human DNA in the chick tissue) were expressed as $\Delta\Delta Ct = \Delta Ct_{\text{control}} - \Delta Ct_{\text{treatment}}$. Relative changes in metastasis were then calculated as $2^{\Delta\Delta CT}$. Each assay included a negative control, a positive control, a no-template control, and the experimental samples in duplicate.

To approximate the actual number of tumor cells present in each tissue sample, a standard curve was generated through quantitative amplification of genomic DNA extracted from a serial dilution of HEp3 cells mixed with individual chick lung homogenates. By interpolating the *alu* signal from experimental samples with the standard curve, the actual number of tumor cells/lung could be determined over a range of 50–100,000 cells/lung. Data processing and statistical analysis were performed using GraphPad Prism (GraphPad Software Inc., San Diego, CA) and Microsoft Excel (Microsoft Corporation, Redmond, WA).

Immunohistochemical and Fluorescent Detection of Metastatic Cells

GFP-expressing tumor cells were visualized *in situ* using whole mounts of tissue harvested from tumor-bearing animals. Whole mounts were prepared by placing the tissue on a glass slide and surrounding it with a bead of vacuum

grease before applying the glass coverslip. Fluorescent tumor cells were observed using standard fluorescent microscopy (Olympus BX60; Olympus, Melville, NY). For IHC staining, each tissue was frozen in Tissue-Tec mounting media (Sakura Finetek, Torrance, CA) and sectioned at 6 μM using a cryostat. Frozen sections were fixed in zinc-formalin for 15 min, rinsed briefly with PBS, and subsequently incubated with blocking buffer (3% BSA in PBS for 2 h) before the addition of primary antibody (2 μg/ml in blocking buffer for 24 h). Specific binding of the primary antibody was detected by the addition of biotin-conjugated goat antimouse antibodies (1 μg/ml for 2 h) followed by peroxidase-conjugated neutravidin (1:500; Pierce, Rockford, IL), which was visualized using 3,3′-Diaminobenzidine (DAB) reagent (Sigma, St. Louis, MO). Each sample was counterstained using Gills hematoxilin (Sigma). Samples were analyzed using transmitted light microscopy (Olympus BX60; Olympus). Digital images were acquired using the C-view imaging software (DVC, Austin, TX) and further processed using Photoshop (Adobe, San Jose, CA).

RESULTS

Quantitative Detection of Human Tumor Cells in Chick Tissue. Chick embryos, when inoculated with 1–5 $\times$ 10^5 HEp3 cells onto their CAM, developed large primary tumors (200–500 mg) within 7 days (Fig. 1). Although the lungs from these tumor-bearing chick embryos did not display any visible metastatic colonies at 7 days (Fig. 2*A*), immunohistochemical analysis of lung tissue with anti-HEp3 antibodies indicated the presence of numerous metastatic foci throughout the tissue (Fig. 2*B*). The rapid spontaneous metastasis of these human tumor cells was confirmed through fluorescent imaging of GFP-producing HEp3 cells, which readily disseminated from the growing primary tumor to form, by day 7, a scattering of metastatic colonies throughout the lung (Fig. 2*C*). Such microscopic analysis of lung metastasis, however, is laborious, often difficult to quantitate, and does not subscribe easily to large numbers of replicate samples. Nonmicroscopic analysis of spontaneous, metastatic dissemination of HEp3 cells in the chick embryo had previously been achieved indirectly through biochemical measurements of *in vivo* passaged secondary organs (26, 30). However, a direct quantitative measurement of metastasis is required for the in-depth analysis of early events in metastasis as well as for observing changes during the temporal progression of metastasis.

Alu repeat DNA sequences are specific to all human cells and are completely absent from chick tissue (33). Kim *et al.* (4) took advantage of this and used *alu* repeat-sequence PCR to monitor the intravasation of human tumor cells into the chick embryo vasculature. We used this feature and designed a real-time PCR-based method for the quantitation of disseminated metastatic human tumor cells based on the real-time amplification of *alu* repeat sequences present within embryonic tissues from tumor-bearing chick embryos. To determine the range and sensitivity of this method, increasing numbers of HEp3 cells (25 to 400,000) were added into a homogenate of single, individual chick embryo lungs. The total genomic DNA was extracted from each of the homogenates, and 30 ng of DNA was subjected to quantitative real-time *alu* PCR. The *alu* threshold cycle (Ct_{alu}), the cycle at which the *alu* PCR product becomes detectable above background signal, was determined at each cell concentration (Fig. 2*D*, *top panel*). *alu* sequences were readily detected from 25 cells/lung up to 400,000 cells/lung and could be quantified over a range extending from 50 to 100,000 cells/lung. Extracted DNA also was subjected to conventional *alu* PCR and agarose gel electrophoresis. This method yielded an increasing amount of a single 224-bp product (*alu*) that was detectable from 400 cells/lung to 100,000 cells/lung but the signal was not linear over this range (Fig. 2*D*, *bottom panel*). Using the real-time assay and plotting Ct_{alu} as a function of the number of cells/lung, a standard curve could be generated with a linear range over 4 log units and a sensitivity of 50 cells/lung, readily allowing for the quantitation of HEp3 cells in chick tissues (Fig. 2*E*). When another human tumor cell (HT1080) was added in increasing numbers to individual chick embryo lungs and the total extracted DNA subjected to real-time *alu* PCR, a similar standard curve was obtained (Fig. 2*E*). The total DNA content of HEp3 and HT1080 differed, possibly because of differing chromosomal content, and, although this could result in a slightly differing magnitude for the two standard curves, the slope and range of the curves for the two cell lines were nearly identical.

To correlate the amount of the *alu* PCR signal (and thereby the amount of human tumor cell metastasis) to the amount of amplified genomic DNA (and thereby the amount of chick tissue), we used the *chGAPDH* gene as an internal control against which the *alu* signal was normalized ($Ct_{\text{chGAPDH}} - Ct_{alu} = \Delta Ct$). The relative amount of metastasis within an experiment is expressed as $2^{\Delta\Delta Ct}$, where $\Delta\Delta Ct = \Delta Ct_{\text{control}} - \Delta Ct_{\text{treatment}}$ (see "Materials and Methods"). A value above 1.0 indicates metastasis above the level of the control, and values below 1.0 indicate a proportional decrease in metastasis. We can, thus, express the level of metastasis both as the number of human cells/lung or as an integral value of metastasis relative to the control. Both measurements are useful because the former provides insight into the actual number of tumor cells found within given tissues, and the latter provides a means by which to project relative changes in metastasis and facilitates the comparison of separate, independent experiments.

Spontaneous Metastasis of Human Tumor Cells Analyzed by Quantitative *alu* PCR. To test the sensitivity and applicability of this assay, we compared the spontaneous dissemination and lung colonization of highly metastatic HEp3 (M+) cells and the low metastatic variant, HEp3 (M−), the malignancy of which is lost on long-term *in vitro* culture (32, 34, 35). In previous investigations, it was not possible to detect tumor cells directly in the lungs of HEp3 (M−) tumor-bearing animals using standard morphometric or enzymatic measurements (29, 31, 32). We used the above-described real-time *alu* PCR to determine directly the number of tumor cells/lung in HEp3 M+ and M− tumor-bearing animals (Fig. 3*A*). Quantitative real-time PCR of chGAPDH was used to verify the presence of equivalent amounts of amplified genomic DNA (Fig. 3*A*, *bottom panel*). These data demonstrated that in excess of 11,000 cells were detected in the lungs of HEp3 M+ tumor-bearing animals, whereas only 1000 cells were detected in the lungs of HEp3 M−- tumor-bearing animals (Fig. 3*B*). Significantly, the 1000 cells in the lungs of the HEp3 M− tumor-bearing animals were easily detected, yielding a Ct_{alu} of 17–19 (Fig. 3*A*), which demonstrated that, even though HEp3 M− cells had

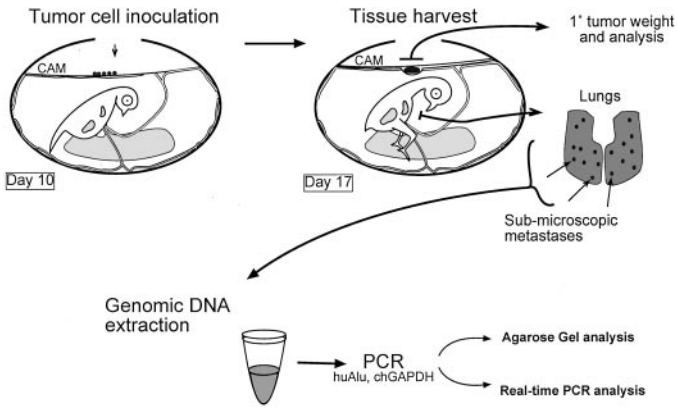

Fig. 1. The chick embryo metastasis model. In the spontaneous metastasis model, human tumor cells are inoculated onto the CAM at embryonic day 10 and allowed to form a tumor by incubating the inoculated eggs for 7 days. At embryonic day 17, the primary tumor and secondary organs such as lung are harvested. Genomic DNA is extracted from the secondary organs and analyzed by conventional or quantitative real-time PCR for the presence of human *alu* repeat sequences and chGAPDH.

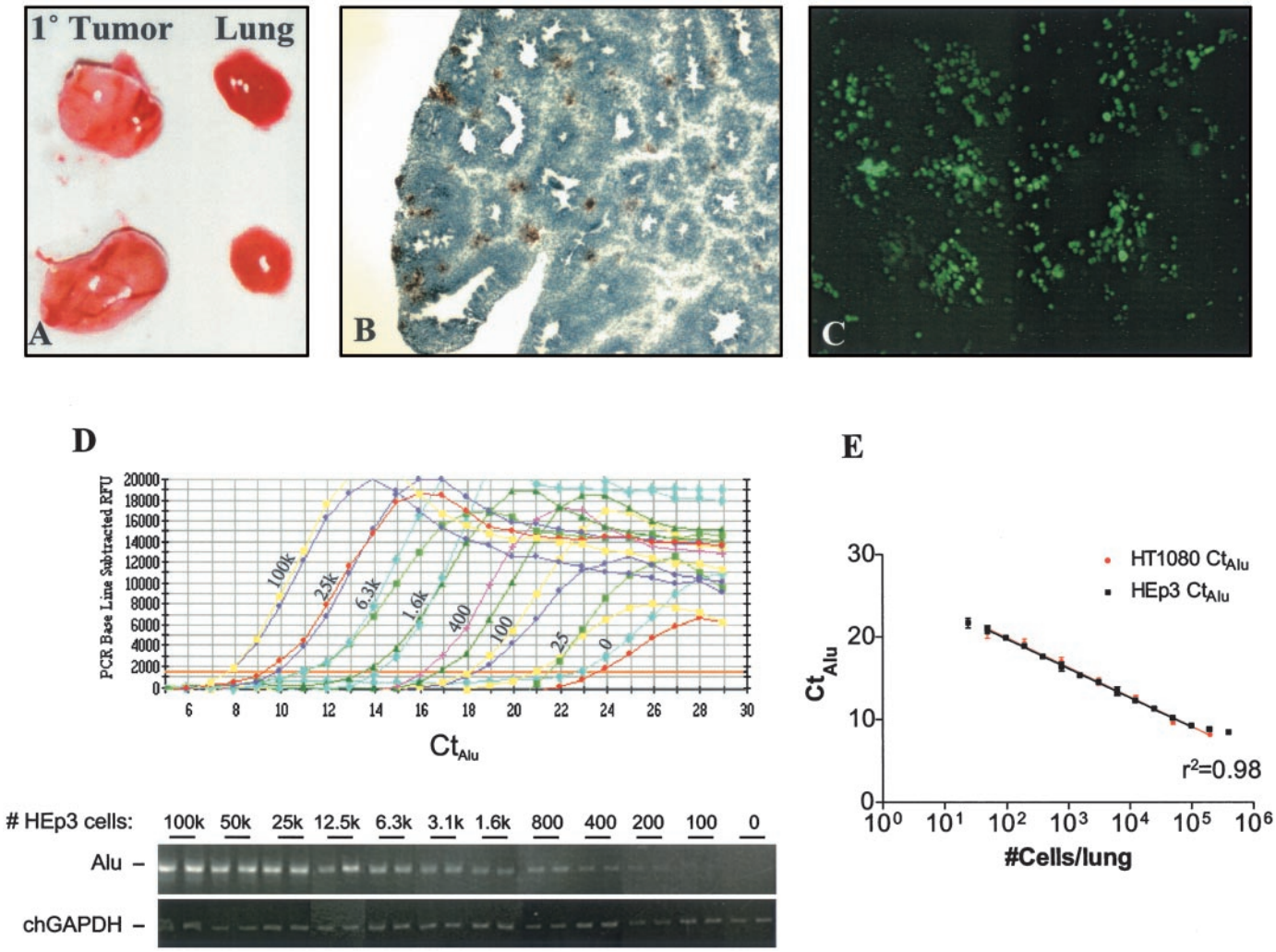

Fig. 2. Detection and quantitation of HEp3 spontaneous metastasis in the chick embryo model. Seven days after 5×10^5 HEp3 cells were placed on the CAM, the newly formed tumor and the embryonic lung were harvested (*A*). Immunohistochemical staining of lung sections with HEp3 specific antibodies (*B*, ×400) or fluorescent microscopic analysis of lung whole mounts containing GFP-expressing HEp3 cells (*C*, ×400) were used to illustrate the metastatic dissemination of HEp3 to the lung. *Alu* PCR was used to amplify *alu* repeat sequences in human (HEp3) DNA. Quantitative real-time *alu* PCR was performed on genomic DNA extracted from the indicated number of HEp3 cells serially diluted into individual chick embryo lung homogenates (*D*, *top panel*). These samples also were analyzed by conventional *alu* and chGAPDH PCR, followed by agarose gel electrophoresis (*D*, *bottom panel*). Real-time quantitative *alu* PCR was used to generate a standard curve from 2.5×10^1 to 4×10^5 HEp3 or HT1080 cells/lung by plotting the *Ct* against the number of cells per lung (*E*). The data are representative of three separate experiments performed in quadruplicate.

significantly reduced metastatic capabilities, a direct measure of their lung metastasis was readily accomplished using quantitative *alu* PCR.

HT1080 fibrosarcoma cells are considered highly malignant cells and are used in many investigations of human tumor-cell invasion and metastasis. HEp3 cells are used by far fewer laboratories but, nevertheless, appear to be distinctly highly malignant both in immunocompromised mice and chick embryos (29, 30, 36). A direct comparison of the malignant, metastatic behavior of HT1080 and HEp3 cells has never been reported. Quantitative *alu* PCR was used to analyze and compare the time- and dose-dependent nature of the spontaneous metastasis of these tumor cells. Both HEp3 and HT1080 are tumor cell lines that readily form well-vascularized primary tumors on the chick embryo CAM and appear to be capable of intravasating into the chick circulation (4). HEp3 M+ was able to spontaneously disseminate from the primary tumor and colonize the lung in a reproducible, dose-dependent manner with as few as 5×10^4 implanted HEp3 cells yielding detectable metastasis (Fig. 4). In contrast, the largest HT1080 tumor cell inoculum onto the CAM (1×10^6 cells) resulted in relatively low levels of spontaneous metastasis, 400 cells/lung. Even though the primary HT1080 CAM tumor size frequently exceeded 500 mg, HT1080 lung metastasis from a 1×10^6 cell inoculum was less than that of the low metastatic HEp3 M− cells arising from only a 5×10^5-cell inoculum (Fig. 4). When equivalent cell inocula (5×10^5) were compared, the extent of HEp3 M+ metastasis was 70-fold higher than HT1080 metastasis for the same period of time (7 days) and from approximately the same primary tumor burden. Although the actual extent and magnitude of HT1080 dissemination to the lung were limited, the observed quantitation of 200–400 cells/lung/7 days was a clear demonstration of the sensitivity of the assay. Furthermore, it also manifested the true spontaneous metastatic ability of the HT1080 because several other human tumor cell lines, including Hs746T and A549 (Fig. 4), were not detected in the lungs of tumor-bearing animals after 7 days of primary tumor growth.

Experimental Metastasis of Human Tumor Cells. There are important aspects of metastasis, such as survival in the vasculature, arrest in the secondary organ, and subsequent secondary growth, that can be directly addressed using the more frequently used experimental metastasis approach (*i.e.*, i.v. delivered tumor cells). The model of experimental metastasis for human tumor cells is mainly carried out in immunodeficient mice. We used *alu* RT-PCR to expand the use of

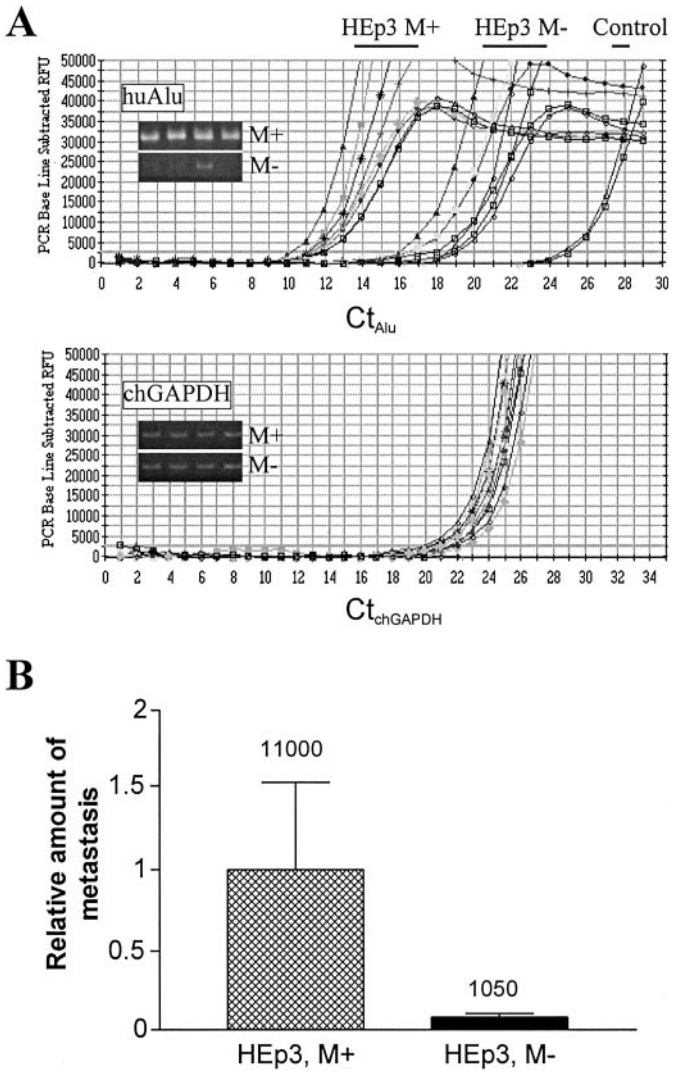

Fig. 3. A comparative analysis of spontaneous metastasis by M+ and M− HEp3 cells. Seven days after placing 5×10^5 M+ and M− HEp3 cells on the CAM of day-10 embryos, the lungs from tumor-bearing animals were harvested and subjected to quantitative real-time *alu* PCR (*A, top panel*). Quantitative real-time PCR of chGAPDH was used to confirm the presence of equivalent quantities of host genomic DNA (*A, bottom panel*). Human *alu* and chGAPDH real-time amplification were compared with conventional PCR in four replicate lung samples (*A,* agarose gel *insets*). In *B,* quantitative detection of HEp3 cells in the embryonic lungs was analyzed, both as the relative amount of metastasis normalized against the amount of host DNA and as the actual number of cells detected per lung (*numbers above the error bars*) calculated from the standard curve in Fig. 2*E*. The data are representative of two consecutive experiments. For each data point, $n \geq 9$.

experimental metastasis in the chick embryo by analyzing the ability of several human tumor cell lines to colonize the embryonic lung after i.v. injection (Fig. 5*A*). The results indicated that 5×10^4 HEp3 cells are much more aggressive in experimental metastasis than other human tumor cell types inoculated at 2×10^5 cells. HT1080 cells, although less experimentally metastatic then HEp3, were substantially more metastatic then some breast carcinoma cell lines (*e.g.,* MDA-MB-435) and lung carcinoma cell lines (*e.g.,* A549). The chick embryo model coupled with the *alu* PCR-based assay was able to clearly distinguish nonmetastatic human tumor cell lines such as HeLa, from the relatively low metastatic cell types such as A549 and MDA-MB-435 (Fig. 5*A*). To confirm that the observed differences between the various numbers of detectable human tumor cells in the lungs (Figs. 4 and 5*A*) were not caused by the widely varying levels of total DNA or *alu* repeats in the different cell types, the following experiment was carried out: Chick embryo lungs were spiked with 1000 cells of each cell type, and total DNA was extracted from the lung/cell mixtures and analyzed by *alu* PCR (Fig. 5*A*, *inset*). The results demonstrated that each cell type yields comparable *alu* signal when extracted from lung tissue.

By taking advantage of the broad quantitative range of *alu* PCR, we also were able to analyze and compare the dose-dependent experimental lung colonization of HEp3 and HT1080. Although experimental lung metastasis was dose dependent for both HEp3 and HT1080, the extent of metastasis was significantly less for HT1080 than for HEp3 (Fig. 5*B*). For equivalent cell injections (2×10^5 cells), experimental metastasis of HT1080 was 8–10 times lower than that of HEp3.

Quantitative Analysis of the Metastatic Cascade. Although it was apparent that HT1080 cells overall were metastatically less efficient than HEp3 cells, from strict end point determinations carried out for the metastasis assays described in Figs. 4 and 5, it was difficult to ascertain what step(s) in the metastatic cascade was (were) rate limiting. To explore possible rate-limiting steps that might differ between the two cell types, we used quantitative *alu* PCR to carry out a temporal analysis of the cascade.

To analyze the progression of tumor cell arrest and lung colonization during experimental metastasis, a time course was performed in which the number of HEp3 and HT1080 cells in the lung was determined at 2 h and at 1, 3, 5, and 7 days after the injection of 1.5×10^5 cells (Fig. 6*A*). This temporal analysis, involving detection of a relatively small number of arrested tumor cells (<1,000) at very early times after injection, and a large number (>50,000) after 5–7 days of growth, was made possible by the sensitivity and quantitative range of real-time a*lu* PCR. From the analysis, it was clear that a small number of HEp3 cells, initially arrested in the lung (~600 cells), begin to proliferate almost immediately, doubling in cell number each day and rapidly expanding over the 7 days to form metastatic colonies approaching 100,000 total cells (Fig. 6*A*). These quantitative measurements were affirmed by microscopic analysis using GFP-expressing HEp3 cells, which were observed to arrest as single cells at 2 h postinjection but subsequently grew to form multicellular colonies (>50 cells/colony) at 7 days postinjection (Fig. 6*B*). The temporal progression of HT1080 cells in experimental lung metastasis was quite different: From the time course (Fig. 6*A*), it is clear that, although an almost equal number of HT1080 and HEp3 cells initially

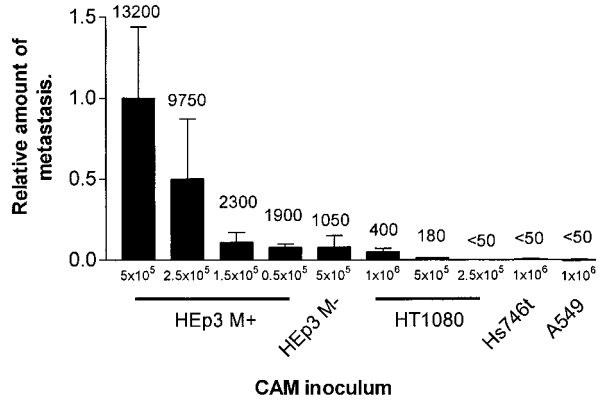

Fig. 4. A quantitative analysis of spontaneous metastasis in the chick embryo using different human tumor cells. Real-time *alu* PCR was used to compare dose-dependent spontaneous metastasis of HEp3 (*M+*) with the metastasis of HEp3 (*M−*), HT1080, Hs746T, and A549 cells. Each indicated tumor cell inoculum was applied topically to the CAM on embryonic day 10, and lungs from tumor-bearing animals were harvested on day 17. Metastasis is presented both as the relative amount of metastasis normalized against chGAPDH and as the actual number of human cells per lung (*numbers above the error bars*). The data are representative of three consecutive experiments. For each data point, $n \geq 5$.

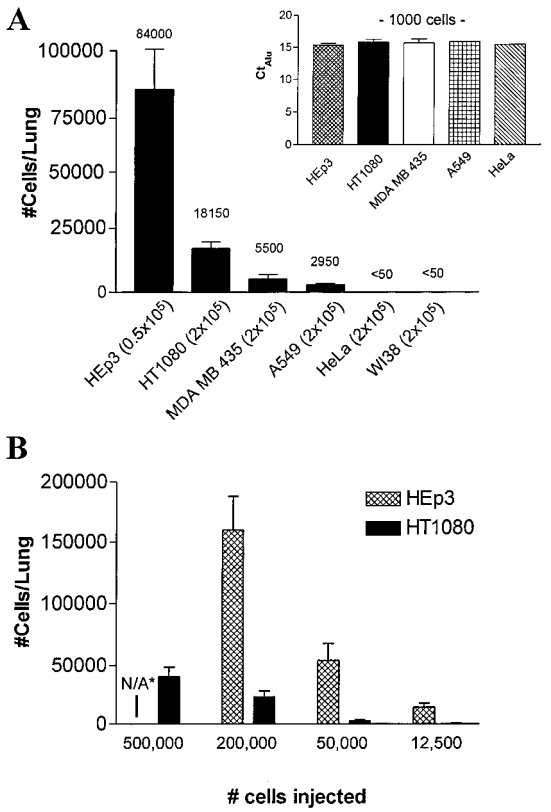

Fig. 5. A quantitative analysis of experimental metastasis in the chick embryo. In *A*, tumor cells were introduced into the chick embryo by injection of the indicated number of cells into the allantoic vein on embryonic day 12. The lungs were harvested on day 19. Total DNA extracted from the harvested lungs was analyzed by real-time *alu* PCR. The number of cells per lung was calculated from the standard curve in Fig. 2*E*. To confirm that each cell type would give comparable detection in chick tissue, lung homogenates, spiked with 1000 cells from each cell type, were processed and analyzed by *alu* PCR to obtain a *Ct alu* value (*A*, *inset*). *B*, a dose-dependent colonization of chick lung by HEp3 and HT1080 was analyzed by real-time *alu* PCR to compare the experimental metastatic capabilities of the two cell types. *N/A**, embryonic death occurred when 5×10^5 HEp3 cells were injected. The data are representative of three consecutive experiments. For each data point, $n \geq 5$.

arrested in the lung (~500–600), the HT1080 cells did not appear to proliferate and expand until much later, because ~1000 HT1080 cells were still present in the lung after 3 days, and ~8000 HEp3 cells were detected at this same point in the time course. This delay in the onset of HT1080 growth resulted after 7 days in a 6-fold reduction overall in HT1080 lung metastasis compared with HEp3 (82,500 HEp3 *versus* 14,800 HT1080). Microscopic observation of GFP-expressing HT1080 cells confirmed that single-cell density for HT1080 cells at 2 h was similar to that of HEp3, and that, after 7 days, the HT1080 multicellular metastatic colonies appeared smaller (Fig. 6*B*). Additional experiments using various numbers of inoculated HT1080 cells confirmed that lung-arrested HT1080 cells clearly manifested a distinct lag in growth initiation, very similar to that shown in Fig. 6*A*, whereas HEp3 cells exhibited no such lag. This resulted in an expanded number of metastatic HEp3 cells that at the 7-day end point is 7–12-fold higher than that of HT1080.

Intravasation during Spontaneous Metastasis. Although delayed initiation of HT1080 growth in the lung accounted for the approximately 10-fold difference in experimental metastasis between the two human malignant cell types, it could not account entirely for the dramatic (60–100-fold) difference between spontaneous metastasis of HEp3 and HT1080 cells (Fig. 4). This discrepancy suggested that, during spontaneous metastasis, HT1080 cells were deficient in an additional rate-limiting step(s) of the metastatic cascade. To further explore other possible rate limiting steps, we used quantitative *alu* PCR to investigate the rate of tumor-cell (HT1080 and HEp3) intravasation.

The appearance of human tumor cells in the tissue and vasculature of the lower CAM was used as a measure of intravasation (4). Primary tumor growth was initiated by inoculating 5×10^5 tumor cells (HEp3 or HT1080) onto the CAMs of 70 embryos. After 3, 5, or 7 days of primary tumor growth, the lower CAMs of 20–30 embryos were excised and analyzed for the presence of intravasated tumor cells (Fig. 7*A*). It would appear that primary tumor growth must reach a critical level before any escaping tumor cells can enter the circulation, because no cells, or few cells (<50), intravasated by day 3 (Fig. 7). However, by day 5, intravasated HEp3 (5,800 cells) and HT1080 (600 cells) were readily detectable in the lower CAM. The 10-fold difference in intravasation between the two malignant cell lines continued into day 7 when 34,700 HEp3 cells and 2,700 HT1080 cells were detected in the lower CAM. These results indicated that under spontaneous metastasis assay conditions, HEp3 cells were escaping from the primary tumor and entering the embryonic circulation (appearing in the lower CAM) at a 10-fold higher rate than HT1080 cells.

It is possible that the observed difference in cell numbers in the lower CAM between HEp3 and HT1080 was not attributable specifically to an intravasation rate but to a differential in arrest or deposition of the two cell types in the lower CAM. It also is possible that similar to the situation in the lung (Fig. 6), there may have been a substantial difference between the two cell types in their growth rate or initiation of growth in the lower CAM that could have contributed partially to the difference in the final number of (growing) cells in the lower CAM that we measured at day 5 and day 7 (Fig. 7*A*). These possibilities could be addressed by carrying out a direct i.v. inoculation of the two cell types and following with time the number of cells

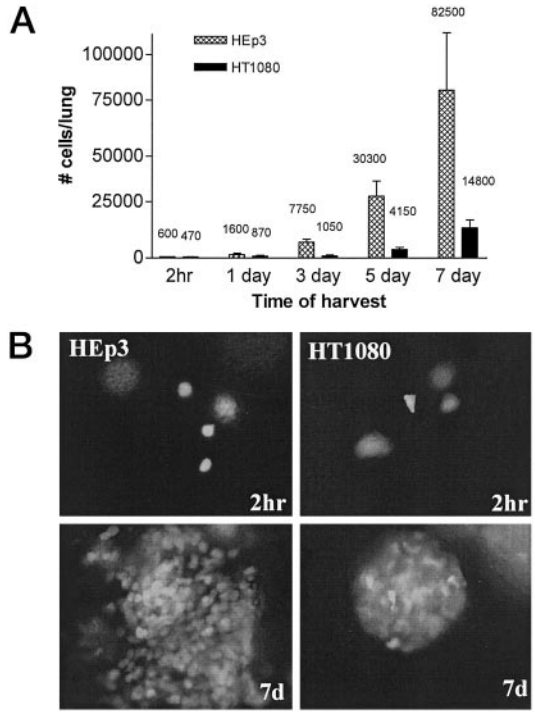

Fig. 6. Growth of arrested cells in the lung during experimental metastasis. An analysis of metastatic growth in the lung during experimental colonization was performed using real-time *alu* PCR of genomic DNA extracted at 2 h and at 1, 3, 5, and 7 days after i.v. injection of 1×10^5 or 2×10^5 HEp3 and HT1080 cells, respectively (*A*). Initial arrest and growth of the tumor cells was confirmed by fluorescent microscopy of GFP-expressing tumor cells during experimental colonization of the chick lung at 2 h and 7 days postinjection (*B*, ×200). For each data point, $n = 5$.

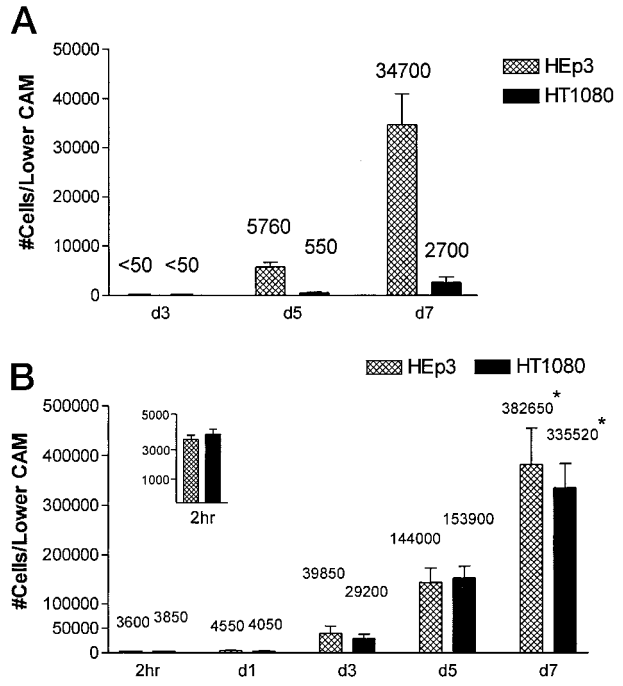

Fig. 7. A quantitative comparative analysis of tumor cell intravasation in the chick embryo. During spontaneous metastasis, the appearance of intravasated tumor cells in the lower CAM was analyzed at 3, 5, and 7 days after the topical inoculation of 5×10^5 tumor cells (*A*). The appearance of tumor cells in the lower CAM was analyzed during experimental metastasis to confirm that HEp3 and HT1080 have equivalent ability to arrest and grow in the lower CAM (*B*). The arrest and growth in the lower CAM was analyzed using quantitative *alu* PCR of genomic DNA extracted at 2 h and at 1, 3, 5, and 7 days after i.v. injection of 1.5×10^5 HEp3 and HT1080 cells. The data presented is a summation of two separate experiments, in which, for each data point, $n \geq 6$ (intravasation) or $n \geq 10$ (growth). *, in *B* at day 7 in the lower CAM, the amount of human *alu* detected exceeds the linear range of the standard curve.

present in the lower CAM. This approach, bypassing the intravasation step, and through the use of the *alu* real-time PCR assay, allows for the accurate measurement in the lower CAM of initially arrested cells and the subsequent growth of those arrested cells. The results of the time course measurements are presented in Fig. 7*B*. At 2 h postinoculation the number of lower CAM-arrested HEp3 cells (3600) was nearly equal to the number of HT1080 arrested cells (3850). At day 1, before any significant cell growth expansion could occur, the number of lower CAM cells for HEp3 and HT1080 remained approximately the same (4500 and 4050, respectively). These results indicated that no new tumor cells had arrived in the lower CAM after 2 h, and, thus, the 2-h value of ~4000 cells each was indeed a true measurement of initial cell arrest. After day 1, both cell types initiated vigorous cell growth because two or three cell divisions appeared to have occurred by day 3 (Fig. 7*B*). In the ensuing 4 days, the HEp3 cells and the HT1080 cells grew and expanded in the lower CAM at approximately equal rates (Fig. 7*B*). Thus, there was no significant difference between HEp3 and HT1080 in the initial tumor cell arrest, in the initiation of cell growth within the lower CAM, or in the overall *in vivo* growth rate of the two cell types. These results ruled out differential arrest and/or differential growth in the lower CAM, and substantiated that there was a 10-fold difference in the spontaneous intravasation rate of HEp3 over HT1080 (Fig. 7*A*).

Rate-limiting Steps in the Metastatic Cascade. Spontaneous metastasis of HT1080 cells was 60–100-fold lower than that of HEp3 cells (Fig. 4) and are likely attributable to a significant deficiency in one or more rate-limiting steps of the metastatic cascade. To determine whether our analysis of the metastatic cascade could account for multiple deficiencies, we expressed all of the acquired quantitative results on HT1080 intravasation, arrest, and growth in secondary tissue as relative values compared with HEp3 cells. In this comparison (Fig. 8), an indication of the identity and relative contribution of those rate-limiting steps became apparent. The 8–10-fold reduction in the intravasation rate of HT1080 was clearly a major contributor to the diminished metastasis of HT1080. In contrast, the strikingly similar efficiency of tumor cell arrest for HT1080 and HEp3, both in the lung and lower CAM, suggested that arrest in the secondary tissue was not rate limiting for HT1080. However, the significant lag in HT1080 growth in the lung accounted for an additional 8–10-fold reduction in the final number of metastatic cells in the lung (Fig. 8). The combination of an 8–10-fold reduction in intravasation with an 8–10-fold reduction in lung secondary growth, predicted a 64–100-fold overall reduction in spontaneous metastasis, very close to the actual observed value (Figs. 8 and 4). Thus, the real-time *alu* PCR method can quantitate individual steps in metastasis and accurately relate their specific contribution to the overall process of spontaneous metastasis.

DISCUSSION

Investigating the metastatic dissemination of human tumor cells requires the use of immunodeficient host animals that can accept xenogeneic transplants. The subsequent detection of a relatively few disseminated human cells in a background of large numbers of xenogeneic host cells, furthermore, requires a sensitive, human-specific monitoring assay. We have combined the accuracy, range, and sensitivity of real-time PCR with the previously demonstrated specificity of *alu* sequences (4) to generate a method that allows for direct quantitative detection of metastatic human cells. Using real-time *alu* PCR, human tumor cells can be detected in the chick embryo lung with as few as 25 cells/lung and can be quantified in a linear range of 50–100,000 cells/lung. The method lends itself easily to both experimental and spontaneous metastasis approaches and is readily applied to most organs and tissues. Furthermore, because it simply uses total

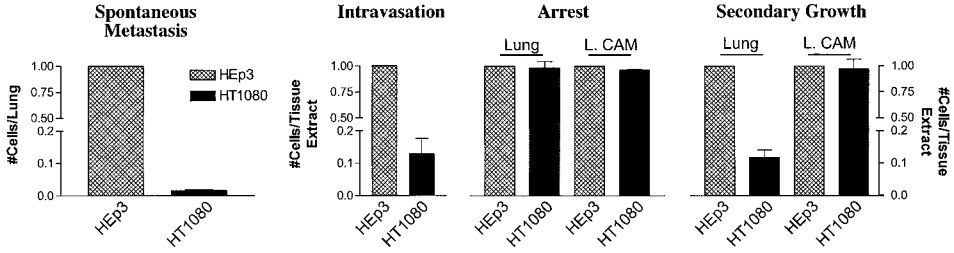

Fig. 8. Relative efficacy of the individual metastatic processes for HT1080 and HEp3. The efficacy by which each cell type intravasates, arrests, and grows within a secondary organ was analyzed, calculated, and presented with the mean value of HEp3 normalized to 1.00. Spontaneous metastasis was quantified by subjecting lung genomic DNA from tumor-bearing animals to *alu* PCR as described in Fig. 4. Genomic DNA extracted from the lower CAMs from the same animals was used to analyze the level of intravasation (as described in Fig. 7*A*). To quantify tumor cell arrest in the lung or the lower CAM (*L. CAM*), each organ was harvested 2 h after i.v. injection of 1.5×10^5 HEp3 or HT1080 cells and subjected to *alu* PCR. Overall growth during experimental colonization by HEp3 and HT1080 cells was assessed by harvesting lungs and L. CAM from animals 7 days after they were given injections of 1.5×10^5 HEp3 or HT1080 cells and subjecting the genomic DNA to *alu* PCR.

DNA extracted from host tissue and requires no additional processing beyond the PCR, a relatively large number of replicate samples (50–100 animals) can be analyzed in a single experiment. In both spontaneous and experimental metastasis assays, *alu* PCR demonstrated that some nonmetastatic and nontransformed human cell lines were incapable of metastasizing to the lung, whereas metastatic cell populations grew exponentially during the duration of the assay. These observations indicate that the detection of *alu* sequences in the lung is a representation of active dissemination of cells and not a passive accumulation of cellular debris. The method, because it monitors *alu* amplification in real-time, is not only sensitive but also extends over a very wide range in cell numbers. This feature allows direct examination of whole organs, assuring the monitoring of an entire metastatic cell population.

Quantitative analysis of metastasis and metastatic processes has been addressed previously by Chambers *et al.* (37) using *in vivo* video microscopy. Such analyses provide the advantage of monitoring individual metastatic cells in tissues for their proliferative or apoptotic state as well as their invasive and migratory behavior (38). In recent years, microscopic approaches using cells expressing GFP have, indeed, provided valuable information on individual steps in the metastatic cascade (5, 39). In some instances video-microscopy can match the quantitation of the PCR-based approaches. However, the *alu* PCR-based method described herein does not require specialized microscopic equipment, is not as labor-intensive as real-time microscopic imaging, and is not limited to those secondary organs and tissues that can accommodate microscopic infiltration. More importantly, the real-time *alu* PCR-based method can very simply provide quantitative information on selective steps in metastasis as they directly relate in the same animal model to the overall efficiency of spontaneous metastasis.

We have taken advantage of the above-described attributes of real-time *alu* PCR to analyze, quantitate, and compare the ability of two human tumor cell types to complete the individual steps in the metastatic cascade. Experimental metastasis, as well as the more challenging process, spontaneous metastasis, have been examined. The two cell types compared were HEp3, a unique, highly metastatic cell that is studied by only a few laboratories, and HT1080, a very well-studied but only a low-to-moderately metastatic human cell type. Both HEp3 and HT1080 form highly vascularized, 200–500 milligram primary tumors on the CAM of the developing chick embryo. However, these two human cell types have never been directly compared in the same metastasis model system. We reasoned that a quantitative study of the two tumor cell types might allow for identification of those cellular properties that convey high metastatic potential, or conversely might allow for elucidation of those distinct characteristics of the low-metastatic cell that negatively regulate aggressive, malignant behavior.

Our initial analysis of spontaneous metastasis demonstrates that HEp3 primary tumor cells disseminate to the lung very efficiently resulting in $1–2 \times 10^4$ cells/lung after 7 days. In contrast, the same size primary cell inoculum of HT1080, results in the metastatic dissemination of only 200–400 cells/lung after 7 days (Fig. 4). Although there is as much as a 100-fold difference in spontaneous metastasis between the two cell types, the sensitivity and extensive range of the real-time *alu* PCR allowed for both of them to be quantified. In contrast to spontaneous metastasis, there is only a 6–10-fold difference between the rate of experimental metastasis of these two cell types (Figs. 5 and 6). This differential between spontaneous and experimental metastasis strongly indicated that, relative to HEp3, HT1080 metastasis encompasses at least two rate-limiting steps. One step appears to be restricted to spontaneous metastasis, and an additional step(s) seems to be associated with postintravasation events integral to experimental metastasis. Primary tumor growth, neovascularization, and intravasation are unique to spontaneous metastasis. However, primary tumor growth and neovascularization were similar for both cell types, and in, fact, HT1080 primary tumors appeared larger and more vascularized than HEp3 tumors.[5] Therefore, intravasation, a key process bypassed by experimental metastasis, was the primary candidate for a rate-limiting step. Kim *et al.* (4) demonstrated that analysis of the lower CAM provides a valid method for monitoring intravasation. When we applied our real-time-based PCR analysis to HEp3 and HT1080 intravasation (Fig. 7), it became quite apparent that intravasation was a rate-limiting process for HT1080 tumor cells. It had long been suggested by Weiss *et al.* (11) that intravasation is one of the critical steps in metastatic dissemination of tumor cells. In fact, several cell lines selected for their metastatic capacity under experimental metastasis conditions were thought to be deficient in intravasation because their metastatic advantage is lost during spontaneous metastasis (9, 40). Kim *et al.* (4) documented that some tumor cells are clearly deficient in intravasation and indicated that the specific proteolytic ability of tumor cells to breach the vascular wall is the critical event in intravasation. More recently, Wyckoff *et al.* (39) used video microscopy to demonstrate that distinct differences in primary tumor cell intravasation can account partially for the significant difference in spontaneous metastasis of two mammary adenocarcinoma cell lines. It was suggested that a chemotactic-like movement of highly metastatic cells toward blood vessels and their ability to avoid fragmentation on intravasation, were critical features.

Our observed 10-fold difference in intravasation rates between HEp3 and HT1080 could indeed be caused by differences in the proteolytic capacity of the two cell types. However, the key proteolytic components for intravasation as indicated by Kim *et al.* (4), MMP-9 and uPA/uPA receptor (uPAR), are expressed by both cell types. Distinct differences in the migratory/invasive properties between HEp3 and HT1080 also can be observed. In analyzing primary tumors and metastatic colonies of GFP-expressing tumor cells, we have observed that HEp3 cells are highly motile within the tissue. Not only do HEp3 cells readily disseminate from the primary tumor into the mesenchyme of the CAM, but they also form lung colonies which are loosely dispersed with little contact between neighboring cells (Figs. 2 and 6). Many single isolated HEp3 cells appear to be migrating away from the main colony. In contrast, most HT1080 colonies are compact with defined borders, suggesting that these cells are less motile and disperse slower within the tissue. Whether these phenotypes are a result of quantitative differences in proteolytic capability or caused by differences in adhesive interactions between the tumor cells and the host tissue microenvironment is unknown but will be the subject of future studies.

The 10-fold differential in intravasation rate between HEp3 and HT1080, although substantial, cannot fully account for the 50–100-fold difference in spontaneous metastasis of the two cell types. It would appear that other rate-limiting steps in the metastatic cascade must be differentially manifested by HEp3 and HT1080. Previous investigations have indicated that selective tumor cell arrest in the microvasculature of the secondary organ is a critical event in metastasis (7, 41, 42).The multiple selecting factors that appear to control tumor cell arrest include platelets, coagulation components, mucins, lectins, integrins, and other molecules on the surface of the arresting tumor cell or the vascular endothelial cell. However, we found no difference in the ability of HEp3 and HT1080 to arrest in either the lung or the lower CAM. The consistent detection of similar quantities

[5] Unpublished observations.

of HEp3 and HT1080 cells during their initial arrival (1–2 h) and during later periods (1–3 days) in the metastatic process, strongly indicates that both cell types have similar rates of arrest. Other studies in both the mouse and chick embryo also indicated that initial tumor cell arrest does not appear to differ significantly between poorly metastatic and highly metastatic cells (15, 43).

In contrast to tumor cell arrest, a time course of tumor cell growth and expansion in secondary tissue indicated that the initiation of growth by arrested HT1080 cells was a critical element of metastatic inefficiency. The actual number of HT1080 cells that arrest in the lung in the first 2 h is maintained for 3 days, whereas HEp3 cells in an identical environment progressively grow and expand (Fig. 6). It is not possible to determine whether the constant number of HT1080 cells over time is a reflection of a balanced proliferation/apoptotic rate, or a reflection of transient HT1080 dormancy. Nevertheless, a clear delay in the expansion of the HT1080 population is observed. This result corresponds with previous work which suggest that the initiation of growth, or lack thereof, by arrested tumor cells is a rate limiting step in metastasis (43). Furthermore, whereas growth initiation is delayed in the lung, no such delay is observed in the lower CAM. This tissue-selective initiation of growth suggests that the microenvironment of the lung is less conducive to initiating HT1080 growth, possibly reflecting the existence of key elements of tissue-specific growth. The long-term failure to initiate growth is known to lead to dormancy of occult tumor cells (12, 44). The survival of dormant tumor cells is of major clinical importance because activation of dormant cells is thought to be the primary cause for relapse of neoplastic disease in treated cancer patients (45, 46). Further insight into the delay of HT1080 growth initiation and its apparent resumption may provide insight into the factors that regulate tissue-specific dormancy of occult tumor cells.

Although metastasis, arrest, growth, and intravasation have been studied in separate investigations and with different models (4, 19, 21, 39, 47–49), this is the first study to quantitatively analyze both spontaneous and experimental metastasis coordinately, as well as to provide a quantitative assessment of the individual steps in the metastatic cascade. The identification of two separate rate-limiting steps in HT1080 metastasis and their relative contribution to spontaneous lung metastasis illustrates that the acquisition of metastatic abilities by a tumor cell is multifaceted and that each step in the metastatic cascade that is "mastered" provides a quantitative contribution to the overall progression of metastasis. Although we have delineated two deficiencies in a low-to-moderately metastatic human tumor cell, HT1080, the study underscores the uniquely and highly efficient metastatic ability of HEp3 cells. This epidermoid carcinoma cell line appears to have no limits to its aggressive behavior. It is rapidly metastatic in chick embryos, in mice, and in the original patient from which it was isolated (50). It intravasates at a high rate and rapidly proliferates in secondary organs. The present investigation and several studies of L. Ossowski [Kim *et al.* (4), Yu *et al.* (16), Ossowski and Reich (34), Ossowski *et al.* (36), Aguirre-Ghiso *et al.* (44), and Ossowski (51)] clearly indicate it to be one of the most highly metastatic human tumor cells available for study. That it is 100-fold more metastatic than the popular and well-studied HT1080 cell line, indicates that HEp3 also is well worthy of further investigation.

Although the chick embryo model and the *alu* PCR detection system lend themselves easily to metastatic HEp3 analysis and with the enhanced sensitivity to HT1080 analysis, a number of other human tumor cell lines did not yield detectable lung metastasis within the 7-day primary tumor growth period. However, if one implants a higher number of primary tumor cells ($>1 \times 10^6$) on the CAM and extends the *in vivo* incubation out to 9 days (the last day before embryo hatching), the detection and quantitation of other metastasizing human tumor cells is feasible. We have now detected in the chick embryo, lung metastasis of the human neuroblastoma cell, SKNBE2, the human colon carcinoma cell, DLD-1, and the human prostate cancer cell, PC3 (data not shown).

The quantitative analysis of rate-limiting steps in metastasis as presented in this study provides critical insight into the relative contribution of individual steps in the metastatic cascade to the overall efficiency of metastasis. This method of investigation can lend itself readily to the investigation and identification of molecular effectors that might diminish the metastasis of highly metastatic cells, such as HEp3, or conversely, facilitate the metastasis of relatively low metastatic cells such as HT1080. Furthermore, when such specific effector molecules are identified, it will be possible to quantitatively address their therapeutic capabilities or targeting potential.

REFERENCES

1. Liotta, L. A., and Stetler-Stevenson, W. G. Principles of molecular cell biology of cancer: cancer metastasis. *In:* DeVita, V. T., Hellman, S., and Rosenberg, S. A. (eds.), Cancer: Principles and Practice of Oncology, pp. 134–149. Philadelphia: J. B. Lippincott, 1993.
2. Fidler, I. Molecular biology of cancer: invasion and metastasis. *In:* V. T. DeVita, S. Hellman, and S. A. Rosenberg (eds.), Cancer principles and practice of oncology, Ed. 5, pp. 135–152. New York: Lippincott-Raven, 1997.
3. Hanahan, D., and Weinberg, R. A. The hallmarks of cancer. Cell, *100:* 57–70, 2000.
4. Kim, J., Yu, W., Kovalski, K., and Ossowski, L. Requirement for specific proteases in cancer cell intravasation as revealed by a novel semiquantitative PCR-based assay. Cell, *94:* 353–362, 1998.
5. Chambers, A. F., Naumov, G. N., Varghese, H. J., Nadkarni, K. V., MacDonald, I. C., and Groom, A. C. Critical steps in hematogenous metastasis: an overview. Surg. Oncol. Clin. North Am., *10:* 243–255, 2001.
6. Woodhouse, E. C., Chuaqui, R. F., and Liotta, L. A. General mechanisms of metastasis. Cancer (Phila.), *80:* 1529–1537, 1997.
7. Felding-Habermann, B., O'Toole, T. E., Smith, J. W., Fransvea, E., Ruggeri, Z. M., Ginsberg, M. H., Hughes, P. E., Pampori, N., Shattil, S. J., Saven, A., and Mueller, B. M. Integrin activation controls metastasis in human breast cancer. Proc. Natl. Acad. Sci. USA, *98:* 1853–1858, 2001.
8. Al-Mehdi, A. B., Tozawa, K., Fisher, A. B., Shientag, L., Lee, A., and Muschel, R. J. Intravascular origin of metastasis from the proliferation of endothelium-attached tumor cells: a new model for metastasis. Nat. Med., *6:* 100–102, 2000.
9. Weiss, L., Mayhew, E., Rapp, D. G., and Holmes, J. C. Metastatic inefficiency in mice bearing B16 melanomas. Br. J. Cancer, *45:* 44–53, 1982.
10. Aukerman, S. L., Price, J. E., and Fidler, I. J. Different deficiencies in the prevention of tumorigenic-low-metastatic murine K-1735b melanoma cells from producing metastases. J. Natl. Cancer Inst. (Bethesda), *77:* 915–924, 1986.
11. Weiss, L. Metastatic inefficiency. Adv. Cancer Res., *54:* 159–211, 1990.
12. Cameron, M. D., Schmidt, E. E., Kerkvliet, N., Nadkarni, K. V., Morris, V. L., Groom, A. C., Chambers, A. F., and MacDonald, I. C. Temporal progression of metastasis in lung: cell survival, dormancy, and location dependence of metastatic inefficiency. Cancer Res., *60:* 2541–2546, 2000.
13. Wong, C. W., Lee, A., Shientag, L., Yu, J., Dong, Y., Kao, G., Al-Mehdi, A. B., Bernhard, E. J., and Muschel, R. J. Apoptosis: an early event in metastatic inefficiency. Cancer Res., *61:* 333–338, 2001.
14. Clark, E. A., Golub, T. R., Lander, E. S., and Hynes, R. O. Genomic analysis of metastasis reveals an essential role for RhoC. Nature (Lond.), *406:* 532–535, 2000.
15. Koop, S., Schmidt, E. E., MacDonald, I. C., Morris, V. L., Khokha, R., Grattan, M., Leone, J., Chambers, A. F., and Groom, A. C. Independence of metastatic ability and extravasation: metastatic ras- transformed and control fibroblasts extravasate equally well. Proc. Natl. Acad. Sci. USA, *93:* 11080–11084, 1996.
16. Yu, W., Kim, J., and Ossowski, L. Reduction in surface urokinase receptor forces malignant cells into a protracted state of dormancy. J. Cell Biol., *137:* 767–777, 1997.
17. Saha, S., Bardelli, A., Buckhaults, P., Velculescu, V. E., Rago, C., St. Croix, B., Romans, K. E., Choti, M. A., Lengauer, C., Kinzler, K. W., and Vogelstein, B. A phosphatase associated with metastasis of colorectal cancer. Science (Wash. DC), *294:* 1343–1346, 2001.
18. Shioda, T., Munn, L. L., Fenner, M. H., Jain, R. K., and Isselbacher, K. J. Early events of metastasis in the microcirculation involve changes in gene expression of cancer cells. Tracking mRNA levels of metastasizing cancer cells in the chick embryo chorioallantoic membrane. Am. J. Pathol., *150:* 2099–2112, 1997.
19. Fidler, I. J., Yano, S., Zhang, R. D., Fujimaki, T., and Bucana, C. D. The seed and soil hypothesis: vascularisation and brain metastases. Lancet Oncol., *3:* 53–57, 2002.
20. Liotta, L. A., and Kohn, E. C. The microenvironment of the tumour-host interface. Nature (Lond.), *411:* 375–379, 2001.
21. Borsig, L., Wong, R., Feramisco, J., Nadeau, D. R., Varki, N. M., and Varki, A. Heparin and cancer revisited: mechanistic connections involving platelets, P-selectin, carcinoma mucins, and tumor metastasis. Proc. Natl. Acad. Sci. USA, *98:* 3352–3357, 2001.
22. Ausprunk, D. H., and Folkman, J. Migration and proliferation of endothelial cells in preformed and newly formed blood vessels during tumor angiogenesis. Microvasc. Res., *14:* 53–65, 1977.

23. Nguyen, M., Shing, Y., and Folkman, J. Quantitation of angiogenesis and antiangiogenesis in the chick embryo chorioallantoic membrane. Microvasc. Res., *47:* 31–40, 1994.
24. Seandel, M., Noack-Kunnmann, K., Zhu, D., Aimes, R. T., and Quigley, J. P. Growth factor-induced angiogenesis *in vivo* requires specific cleavage of fibrillar type I collagen. Blood, *97:* 2323–2332, 2001.
25. Vogt, P. K., Aoki, M., Bottoli, I., Chang, H. W., Fu, S., Hecht, A., Iacovoni, J. S., Jiang, B. H., and Kruse, U. A random walk in oncogene space: the quest for targets. Cell Growth Differ., *10:* 777–784, 1999.
26. Ossowski, L., and Reich, E. Experimental model for quantitative study of metastasis. Cancer Res., *40:* 2300–2309, 1980.
27. Chambers, A. F., Shafir, R., and Ling, V. A model system for studying metastasis using the embryonic chick. Cancer Res., *42:* 4018–4025, 1982.
28. MacDonald, I. C., Schmidt, E. E., Morris, V. L., Chambers, A. F., and Groom, A. C. Intravital videomicroscopy of the chorioallantoic microcirculation: a model system for studying metastasis. Microvasc. Res., *44:* 185–199, 1992.
29. Brooks, P. C., Lin, J. M., French, D. L., and Quigley, J. P. Subtractive immunization yields monoclonal antibodies that specifically inhibit metastasis. J. Cell Biol., *122:* 1351–1359, 1993.
30. Gordon, J. R., and Quigley, J. P. Early spontaneous metastasis in the human epidermoid carcinoma HEp3/chick embryo model: contribution of incidental colonization. Int. J. Cancer, *38:* 437–444, 1986.
31. Ossowski, L., and Reich, E. Loss of malignancy during serial passage of human carcinoma in culture and discordance between malignancy and transformation parameters. Cancer Res., *40:* 2310–2315, 1980.
32. Testa, J. E. Loss of the metastatic phenotype by a human epidermoid carcinoma cell line, HEp-3, is accompanied by increased expression of tissue inhibitor of metalloproteinase 2. Cancer Res., *52:* 5597–6603, 1992.
33. Kariya, Y., Kato, K., Hayashizaki, Y., Himeno, S., Tarui, S., and Matsubara, K. Revision of consensus sequence of human Alu repeats—a review. Gene (Amst.), *53:* 1–10, 1987.
34. Ossowski, L., and Reich, E. Changes in malignant phenotype of a human carcinoma conditioned by growth environment. Cell, *33:* 323–333, 1983.
35. Nielsen-Preiss, S. M., and Quigley, J. P. Detection and characterization of low abundance cellular proteins that specifically increase upon loss of the metastatic phenotype. J. Cell Biochem., *51:* 219–235, 1993.
36. Ossowski, L., Russo, H., Gartner, M., and Wilson, E. L. Growth of a human carcinoma (HEp3) in nude mice: rapid and efficient metastasis. J. Cell Physiol., *133:* 288–296, 1987.
37. Chambers, A. F., MacDonald, I. C., Schmidt, E. E., Koop, S., Morris, V. L., Khokha, R., and Groom, A. C. Steps in tumor metastasis: new concepts from intravital videomicroscopy. Cancer Metastisis Rev., *14:* 279–301, 1995.
38. Naumov, G. N., Wilson, S. M., MacDonald, I. C., Schmidt, E. E., Morris, V. L., Groom, A. C., Hoffman, R. M., and Chambers, A. F. Cellular expression of green fluorescent protein, coupled with high-resolution *in vivo* videomicroscopy, to monitor steps in tumor metastasis. J. Cell Sci., *112:* 1835–1842, 1999.
39. Wyckoff, J. B., Jones, J. G., Condeelis, J. S., and Segall, J. E. A critical step in metastasis: *in vivo* analysis of intravasation at the primary tumor. Cancer Res., *60:* 2504–2511, 2000.
40. Hamada, J., Takeichi, N., and Kobayashi, H. Metastatic capacity and intercellular communication between normal cells and metastatic cell clones derived from a rat mammary carcinoma, Cancer Res., *48:* 5129–5132, 1988.
41. Orr, F. W., and Wang, H. H. Tumor cell interactions with the microvasculature: a rate-limiting step in metastasis. Surg. Oncol. Clin. North Am., *10:* 357–381, ix-x, 2001.
42. Borsig, L., Wong, R., Hynes, R. O., Varki, N. M., and Varki, A. Synergistic effects of L- and P-selectin in facilitating tumor metastasis can involve non-mucin ligands and implicate leukocytes as enhancers of metastasis. Proc. Natl. Acad. Sci. USA, *99:* 2193–2198, 2002.
43. Luzzi, K. J., MacDonald, I. C., Schmidt, E. E., Kerkvliet, N., Morris, V. L., Chambers, A. F., and Groom, A. C. Multistep nature of metastatic inefficiency: dormancy of solitary cells after successful extravasation and limited survival of early micrometastases. Am. J. Pathol., *153:* 865–873, 1998.
44. Aguirre-Ghiso, J. A., Liu, D., Mignatti, A., Kovalski, K., and Ossowski, L. Urokinase receptor and fibronectin regulate the ERK(MAPK) to p38(MAPK) activity ratios that determine carcinoma cell proliferation or dormancy *in vivo*. Mol. Biol. Cell, *12:* 863–879, 2001.
45. Meltzer, A. Dormancy and breast cancer. J. Surg. Oncol., *43:* 181–188, 1990.
46. Kell, M. R., Winter, D. C., O'Sullivan, G. C., Shanahan, F., and Redmond, H. P. Biological behaviour and clinical implications of micrometastases. Br. J. Surg., *87:* 1629–1639, 2000.
47. Testa, J. E., Brooks, P. C., Lin, J. M., and Quigley, J. P. Eukaryotic expression cloning with an antimetastatic monoclonal antibody identifies a tetraspanin (PETA-3/CD151) as an effector of human tumor cell migration and metastasis. Cancer Res., *59:* 3812–3820, 1999.
48. Chambers, A. F., MacDonald, I. C., Schmidt, E. E., Morris, V. L., and Groom, A. C. Clinical targets for anti-metastasis therapy. Adv. Cancer Res., *79:* 91–121, 2000.
49. Urquidi, V., Sloan, D., Kawai, K., Agarwal, D., Woodman, A. C., Tarin, D., and Goodison, S. Contrasting expression of thrombospondin-1 and osteopontin correlates with absence or presence of metastatic phenotype in an isogenic model of spontaneous human breast cancer metastasis. Clin. Cancer Res., *8:* 61–74, 2002.
50. Toolan, H. W. Transplantable human neoplasms maintained in cortisone treated laboratory animals: HS #1; H. Ep. #1; H. Ep. #3; and H. Emb. #1. Cancer Res., *14:* 660–666, 1954.
51. Ossowski, L. Invasion of connective tissue by human carcinoma cell lines: requirement for urokinase, urokinase receptor, and interstitial collagenase. Cancer Res., *52:* 6754–6760, 1992.